Acido-basicity of lanthana/alumina catalysts and their activity in ethanol conversion

Gabriella Garbarino [a,b,*], Chongyang Wang [b], Ioannis Valsamakis [b,1], Sahar Chitsazan [a], Paola Riani [c], Elisabetta Finocchio [a], Maria Flytzani-Stephanopoulos [b], Guido Busca [a]

[a] Università degli Studi di Genova, Dipartimento di Ingegneria Civile, Chimica e Ambientale (DICCA), Laboratorio di chimica delle superfici e catalisi, P.le Kennedy, 1 16129 Genova, Italy
[b] Department of Chemical And Biological Engineering, Tufts University, Medford, MA,USA
[c] Università degli Studi di Genova, Dipartimento di Chimica e Chimica Industriale (DCCI), Via Dodecaneso, 31 16146 Genova, Italy

ABSTRACT

Lanthana on alumina samples (0.2, 0.8 and 4.7 theoretical monolayers) were prepared by incipient wetness impregnation using γ-Al_2O_3 as support. Characterization has been performed by BET, XRD, skeletal FT-IR, DR-UVvis, XPS, HR-TEM, IR spectra of the surface OH, adsorbed pyridine and CO_2, and isopropanol TPD. Ethanol conversion was investigated both in temperature-programmed surface reaction (TPSR) dynamic conditions as well as in steady-state flow reactor tests. Lanthanum addition stabilizes alumina with respect to sintering and loss of surface area and La- containing phases are observed only for the high-La loaded catalyst. La-alumina catalysts are less active in ethanol dehydration than alumina but more selective to diethyl ether at partial conversion. $5\%La_2O_3/Al_2O_3$ is also equally or more selective than alumina to ethylene at high conversion, producing less carbonaceous material during reaction. Thus, this catalytic system might be a good candidate for (bio)ethylene production through (bio)ethanol dehydration.

© 2016 Elsevier B.V. All rights reserved.

1. Introduction

Lanthanum oxide is reported to be an excellent basic catalyst for a number of reactions [1]. In contrast, alumina is considered an excellent Lewis acid catalyst [2]. The addition of lanthanum is known to stabilize alumina for high temperature applications [3,4], such as catalytic combustion [5]. This is one of the reasons that La_2O_3 is included in the composite CeO_2-ZrO_2-La_2O_3-Al_2O_3 washcoats used to support noble metal catalysts in catalytic converters for gasoline engine cars [6] as well as in catalyzed diesel particulate filters [7,8].

La_2O_3 addition was also found to improve catalytic activity, stability and resistance to coking of a number of alumina supported metal catalysts such as Ni/Al_2O_3 catalysts for the steam reforming of ethanol [9,10] steam reforming of biomass tars [10], dry reforming of methane [11] and steam gasification of biomass [12].

"Second generation bioethanol", i.e. ethanol produced by fermentation of lignocellulosics, could become a primary intermediate in the frame of a new chemical technology industry based on renewables [13,14]. Among the secondary intermediates potentially obtainable by converting (bio)ethanol, ethylene and diethyl ether can be obtained by catalytic dehydration. One of the best catalysts for these reactions is γ-Al_2O_3 [15,16], which allows yields of the order of 70–75% in diethylether at ca 473 K and almost total yield in ethylene at temperatures in the range 573–623 K. Previous studies have shown that the performance of alumina, although very good, is limited by the production of small amounts of higher hydrocarbons [16–19]. A main point, additionally, is catalyst stability, due to the growth of carbonaceous materials that may progressively poison the catalyst [19]. Both phenomena might be due, at least in part, to acid-catalyzed overconversion of ethylene. Thus, doping of alumina with basic components could be beneficial. On the other hand, catalysts with basic and/or redox properties catalyse the conversion of (bio)ethanol to a number of other relevant chemicals, such as acetaldehyde, acetone, butenes, butadiene, etc. [20,21].

To shed light into the chemistry of ethanol on oxide surfaces, we investigated its conversion over alumina modified by lanthana in parallel with the surface acido-basicity of this system. The aim of this investigation is dual: i) to look at the effect of lanthanum

---

doping on the acidic properties of alumina and its performance in ethanol dehydration; and ii) to look at the effect of lanthanum-rich catalysts, supposed to be moderately basic, on ethanol conversion.

2. Experimental

2.1. Materials preparation

Catalysts were prepared using Puralox 200 Sba (γ-Al$_2$O$_3$, 200 m^2/g) from Sasol previously calcined at 1023 K for 5 h as bare support. The catalytic materials, summarized in Table 1, were prepared through incipient wetness impregnation using La(NO$_3$)$_3$*xH$_2$O (x~4) (from Alfa Aesar) aqueous solutions. The theoretical amounts of La precursor to obtain 5%, 20% and 80% oxide on alumina (measured as 100*wt$_{La2O3}$/wt$_{Al2O3}$ was dissolved in a volume of deionised water such that the total liquid volume was equal to the pore volume of the material. A step of drying at 353 K in vacuum was undertaken for 15 h and calcination in air at 1023 K for 5 h (with a heating rate of 2 K/min) was performed. The sample notation adopted is: A alumina, xLaA for La containing catalysts with x the loaded lanthana weight percent as previously defined.

2.2. Materials characterization

Surface area measurements were performed using a Micromeritics Autochem 2920 with a single point method. The samples were previously pretreated in He at 523 K in order to desorb or decompose potentially adsorbed surface species.

X-Ray diffraction patterns were recorded using Cu Kα radiation (λ = 0.15406 nm). XRD analysis of the fresh catalysts was performed on a Rigaku Smartlab Cu-source powder diffractometer. Cu Kα radiation was used with a power setting of 45 kV and 200 mA. Scan rate of 2°/min with a 0.02° step size was used. Powder patterns were indexed by comparing experimental results to the data reported in the Pearson's Crystal Data database [22].

FTIR studies were performed on compacted powder disks of 15–30 mg activated in vacuum at 773 K before adsorption experiments. CO$_2$ (several Torr) was adsorbed at room temperature (r.t.) and spectra were recorded in the presence of the gas and after outgassing at room temperature and at increasing temperature. Pyridine (5 Torr) was put in contact with the catalysts for ten minutes and then outgassed at different temperatures (473–773 K). In all cases, a Nexus ThermoNicolet instrument was used (OMNIC software, DTGS detector, 100 scans). All the spectra are reported in common scale.

DR-UV-vis-NIR spectra were collected with a JASCO V570 instrument equipped with an integrating sphere.

X-ray photoelectron spectroscopy (XPS) was conducted by using the Thermo Scientific monochromatic Al Kα line (1.4866 keV) as the excitation source. Binding energies were measured on a multi-channel detector with pass energy of 50 eV and energy step of 0.05 eV for high-resolution scans and 0.5 eV for survey scans. Spectral regions are O1s, Al2p and La3d. All the spectra were referenced to the elemental carbon at binding energy (BE) of 284.8 eV. Quantitation of surface components was based on peak fitting and normalization of O (1s), La (3d 5/2), and Al (2p) primary peaks.

High-resolution transmission electron microscopy (HR-TEM) was conducted on a JEOL 2010 electron microscope with 200 kV and 110 μA beam emission.

SEM-EDX characterization was performed in a scanning electron microscope (SEM) EVO 40 (Carl Zeiss SMT Ltd, Cambridge, England) equipped with a Pentafet Link Energy Dispersive X-ray Spectroscopy (EDXS) system managed by the INCA Energy software (Oxford Instruments, Analytical Ltd., Bucks, U.K.) to evaluate composition of the overall samples. Quantitative EDX analysis was

carried out using an acceleration voltage of 20 kV and a counting time of 50 s, using a cobalt standard in order to monitor the beam current, gain and resolution of the spectrometer.

Isopropanol temperature-programmed desorption tests (IPA-TPD) have been performed using a Micromeritics Autochem 2920. Prior to IPA-TPD, the samples (0.11 g) were pretreated in helium at 523 K (heating rate 15 K/min, hold 30 min) in order to remove moisture. Saturation with isopropanol was carried out at room temperature by flowing 30 ml$_{He}$/min in a bubbler for 1 h, followed by a complete purging with He (30 ml/min) for 1 h. TPD was then carried out flowing 30 ml$_{He}$/min and increasing temperature at 5 K/min: products were continuously acquired using a mass spectrometer.

2.3. Catalytic experiments

Temperature programed surface reaction (TPSR) dynamic experiments with ethanol were done with 0.1 g of catalysts diluted in 0.2 g quartz beads by varying the temperature from RT to 973 K in 4 h and holding at that temperature for 10 min. The flow rate was set at 50 ml/min and the ethanol concentration was 7.9% (% v/v) fed with a syringe pump. The analysis of the product gas was done with a mass spectrometer following sixteen different m/z values. To obtain a quantitative measurement, a three point calibration was done for each evolved species. Moreover, a complete analysis was done in order to separate the overlap between signals, thus obtaining quantitative results (mol/mol, %).

Catalytic experiments were performed at atmospheric pressure in a tubular flow reactor (i.d. 6 mm) using 0.500 g catalyst (60–70 mesh sieved, thus achieving a ratio between the particle and internal reactor diameter near 25) and feeding ethanol (96% assay, from Sigma Aldrich) in nitrogen with 11.6 h^{-1} WHSV (total flow rate of 80 cc/min). The carrier gas (nitrogen) was passed through a bubbler containing ethanol maintained at constant temperature (298 K) in order to obtain the desired partial pressures. The temperature in the experiment was varied stepwise from 423 K to 773 K.

Ethanol conversion is defined as usual:

$$X_{EtOH} = (n_{EtOH(in)} - n_{EtOH(out)})/n_{EtOH(in)}$$

While selectivity to product i is defined as follows:

$$S_i = n_i/(\nu_i(n_{EtOH(in)} - n_{EtOH(out)}))$$

where n_i is the moles number of compound i, and ν_i is the ratio of stoichiometric reaction coefficients.

The outlet gases were analyzed by a gas chromatograph (GC) Agilent 4890 equipped with a Varian capillary column "Molsieve 5A/Porabond Q Tandem" and TCD and FID detectors in series. In order to identify the compounds of the outlet gases, a GC–MS Thermo Scientific with TG-SQC column (30 m $\times$ 0.25 mm $\times$ 0.25 μm) was used.

2.4. Temperature programmed oxidation of spent catalysts

Temperature programmed oxidation (O$_2$-TPO) was carried out mixing 0.150 g of the spent catalyst with 0.500 g of sand (purchased from Sigma-Aldrich and calcined at 1073 K for 6 h prior to use). A mixture of 10% oxygen and 90% nitrogen was fed to the reactor, while temperature was raised from 298 K up to 1123 K with a heating rate of 10 K/min. The outlet gases were collected online using a gas cell and an IR spectrometer (ThermoNicolet Instrument). Prior to each TPO experiment, an accurate background was collected with the same flow rate in pure N$_2$. For CO$_2$ and CO the signals at 2341 cm^{-1} (CO$_2$ asymmetric stretching) and 2170 cm^{-1}, respectively, were used as diagnostic bands.

Table 1
Sample notation and surface area of fresh samples[a].

Sample	%La$_2$O$_3$100*w$_{La2O3}$/w$_{Al2O3}$	mol$_{La2O3}$/mol$_{Al2O3}$	S$_{BET}$ [m^2/g$_{CAT}$]	S$_{BET}$ [m^2/g$_{Al2O3}$]	Å^2 $_{Al2O3}$/at$_{La}$	at$_{La}$/nm^2 $_{Al2O3}$	Theoretical monolayer fraction[b]
A	0	0	170	170	–	0	0
5LaA	5	0.015	174	183	99	1.01	0.2
20LaA	20	0.062	151	181	24.5	4.08	0.8
80LaA	80	0.25	67	121	4.1	24.4	4.7

[a]Calcined in air at 1023 K, 5 h.

[b] Assuming 5.2 La atoms per nm^2 of alumina as the monolayer coverage [53].

3. Results

3.1. Characterization of the fresh catalysts

3.1.1. Surface area measurements

The surface areas of the catalysts are summarized in Table 1. The surface area of the pure alumina support decreases upon calcination (1023 K for 5 h) from 200 m^2/g to 170 m^2/g. Lanthanum addition does not significantly affect the 5LaA and 20LaA surface areas, while it affects significantly the 80LaA one.

3.1.2. X-Ray diffraction (XRD)

In Fig. 1, the XRD patterns of the samples under study are reported. The XRD pattern of the A support presents the pattern of γ-alumina, assumed to be a nearly cubic non-stoichiometric spinel [23]. In the cases of the 5LaA and 20LaA samples, the alumina's XRD pattern is also present although significantly weakened. In the case of the 80LaA sample, alumina peaks are still present even if very weak, while sharp peaks are observed characteristic of the LaAlO$_3$ and the La(OH)$_3$ phases [22,24].

3.1.3. Skeletal IR and UV–vis spectroscopic characterization

The alumina spectrum (A) confirms the results obtained by XRD showing the typical features of γ-Al$_2$O$_3$ [23] (Fig. 1S). An analogous spectrum is observed for both 5LaA and 20LaA, thus confirming that the interaction of La species with the alumina bulk is small, if any, in these samples, as also suggested by the XRD patterns. The spectrum of 80LaA is definitely modified, with the additional formation of two sharp features at 646 and 418 cm^{-1}. In the OH stretching region this sample also shows a sharp band at 3609 cm^{-1} and a broad absorption at 3446 cm^{-1}, which correspond well to those reported for La(OH)$_3$ [25].

The diffuse reflectance UV–vis and Near Infrared spectra (DR-UV–vis-NIR) of the catalysts are reported in Fig. 2S. The weak absorption in the UV region is typically associated with charge transfer transitions that gives rise in bulk oxides to bandgap transition. It is well-known that alumina is an insulator and its bandgap transition falls in the far-UV, i.e. at higher energy outside the range available with our instrument. A weak absorption observed in the spectrum of LaA samples at 280 nm in the near-UV region is likely associated to O^{2-} (2p) → La^{3+} charge transfer.

3.1.4. TEM microscopic study

The TEM micrographs of the four as prepared samples under study are shown in Fig. 2. The alumina sample shows nanoparticles characterized mainly by a prismatic shape, with 10–30 nm length and 5–15 nm width. The particle shape for 5LaA looks similar, while the shape of particles in the 20LaA sample is more rounded. Darker small particles are also apparent, likely due to La-rich material. The particle shape in the case of 80LaA is definitely different, with a more rounded shape and many small spherical La-rich particles. The average size of the La particles in 80LaA is 1.36 nm by counting 85 particles in the HRTEM image of 80LaA. In this case, alumina serves as a dispersant of the La-rich phase in the LaA mixtures with high La concentration.

3.1.5. Surface characterization with X-Ray photoelectron spectroscopy

In Fig. 3, the XP spectra of the catalysts are reported in the O(1s), Al(2p) and La(3d5/2) regions. In the case of alumina, as usual, the O(1s) signal is split, with a contribution near 530 eV that is assigned to oxide species and a second contribution at higher energy that is assigned to hydroxide species [26]. The Al(2p) signal is single at 73.9 eV, as usual for γ-Al$_2$O$_3$ [27,28], confirming that this technique cannot distinguish among different coordinations of surface Al^{3+} ions. The O(1s) and Al(2p) spectra are not significantly perturbed by lanthanum addition in the case of 5LaA and 20LaA, in agreement with previous studies [29,30]. However, the Al(2p) signal shifts slightly at higher energy while the O(1s) signal shifts slightly to lower energies.

The peaks observed in the lanthanum 3d5/2 transition can be deconvoluted as due to two doublets in all cases. This splitting is a consequence of two different final states in the photon emission, and as a result of hybridization of 4f orbitals of La atoms with surrounding atoms (3d^{9}4f^1 and 3d^{9}4f^0 final states, for higher and lower binding energy peaks, respectively). The peak positions are reported in Table 1S while in Table 2 atomic composition from design, XP spectra and EDX are summarized for each sample with data in good agreement. In the case of 80LaA, a great variation in composition was obtained during the EDX analysis, thus confirming the presence of La- rich particles that were almost absent in all other samples.

In 5LaA and 20LaA samples, the higher energy doublets are found at slightly higher energies than those reported for bulk La(OH)$_3$ [31] and, even more, than those reported for La$_2$O$_3$ [31–33] LaAlO$_3$ [31,33] and a number of La hexaaluminates [34–36]. The peak position in our spectra is even more shifted to higher energies than those reported for other La/Al$_2$O$_3$ samples [33]. As reported by Ferrandon and Björnbom [31], the La 3d5/2 signal is found at slightly higher energy for dispersed La^{3+} than for stoichiometric compounds. This finding supports the idea that La disperses on the surface of alumina on the 5LaA and 20LaA samples without forming compound structures. Concerning the C1s signal, carbonate signal is detectable for all the samples characterized. For A, 5LaA and 20LaA a weak feature in the range 288–290 eV is detectable and assigned to metal carbonates, while only for 80LaA a more complex feature is observed in the region 284–292 eV.

XP spectra of 80LaA provide evidence for a strong perturbation of the surface. In this case, both O(1s) and Al(2p) peaks are strongly split, with components at very high, quite unusual, energy that might be assigned to Al$_2$(CO$_3$)$_3$. A similar behaviour is observed for higher energy La 3d5/2 found at very high energy.

3.1.6. Surface characterization by IR spectroscopy

The spectra of the A, 5LaA and 20LaA samples after activation in vacuum at 773 K in the OH stretching region are reported in Fig. 4 left. The spectrum of A shows the main bands at 3770, 3728 and 3685 cm^{-1}, with an additional shoulder near 3790 cm^{-1}, typical of the surface OHs of γ-Al$_2$O$_3$ [2,37]. The intensity of the massive peak due to OH stretching bands of free surface OH groups decreases significantly by the addition of lanthana. The spectrum
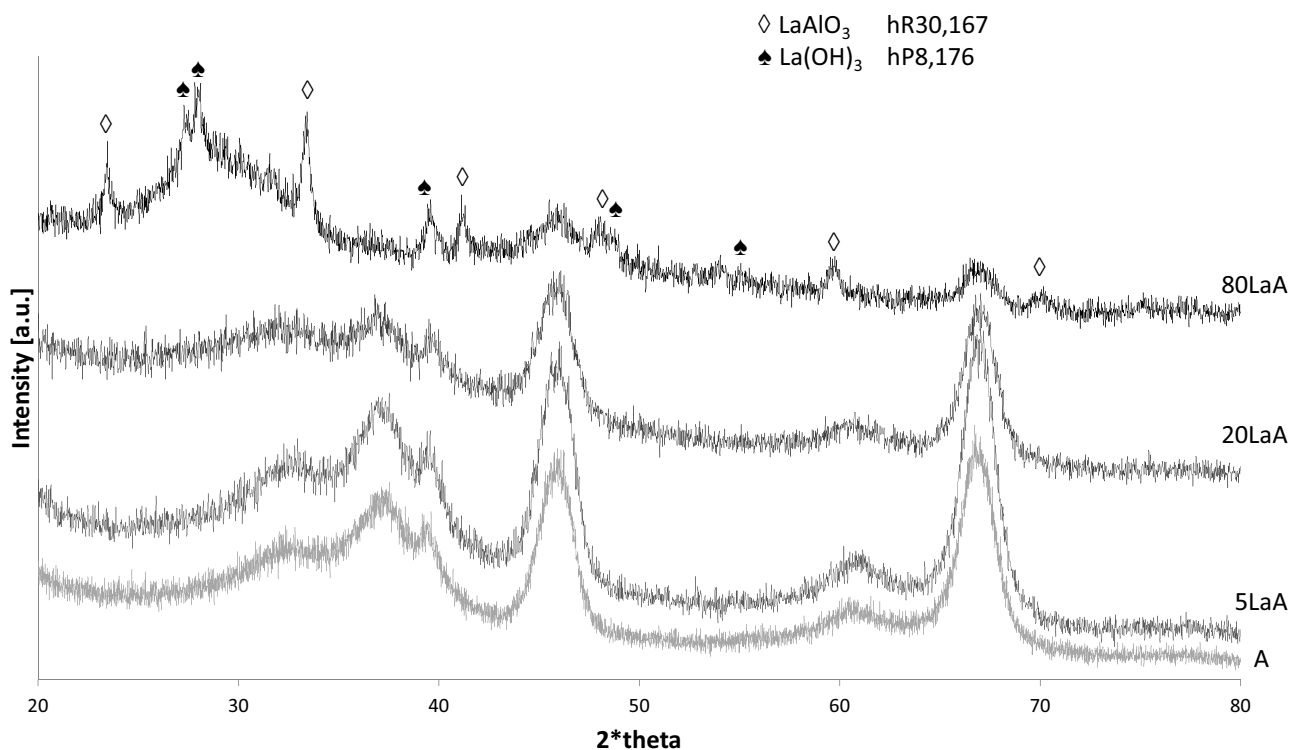
Fig. 1. XRD of the investigated samples and crystalline phase assignments: ◊ LaAlO₃ ♠ La(OH)₃.
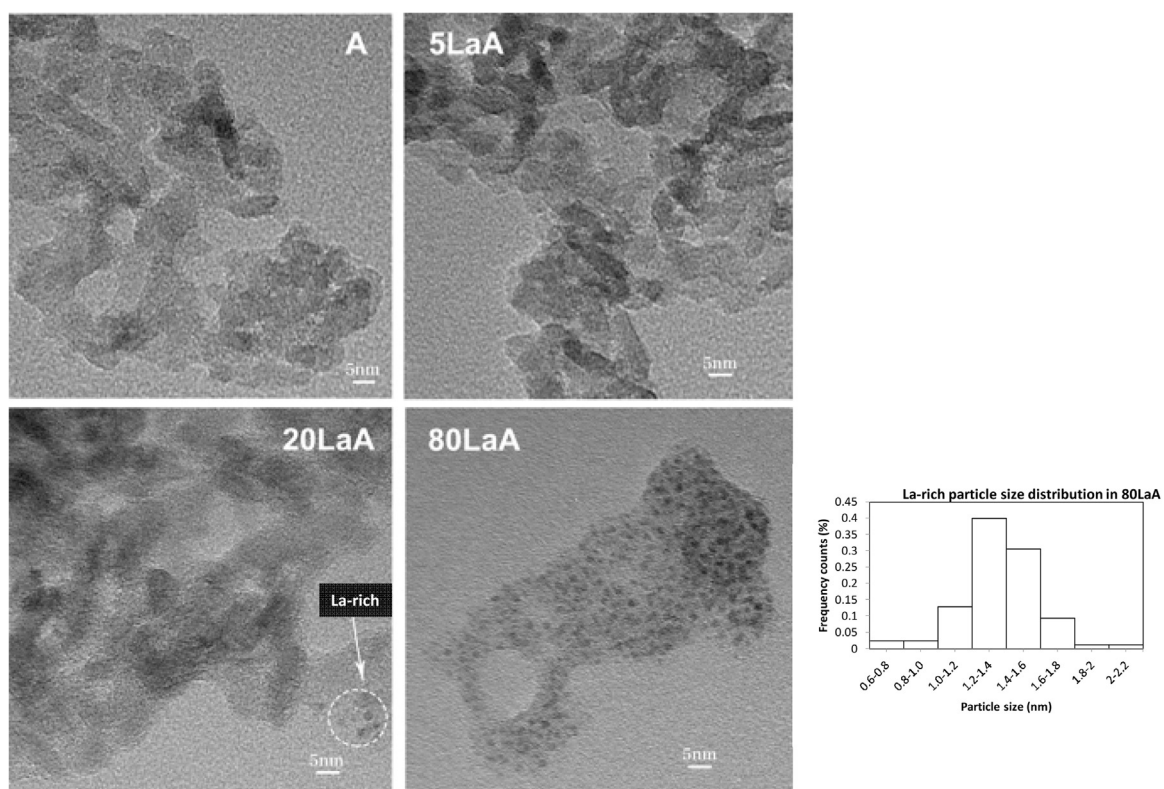

Fig. 2. TEM micrographs of the investigated samples. In the inset of 80LaA micrograph the particle size of La-rich particles is depicted.
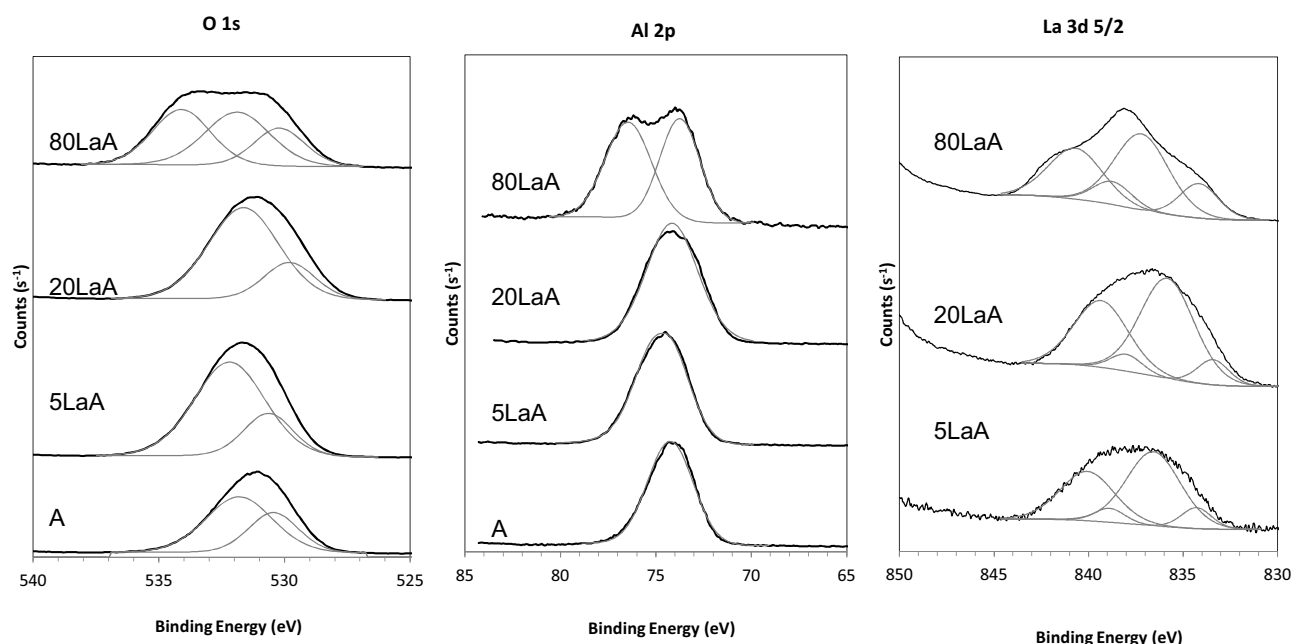
Fig. 3. XP spectra of investigated catalysts are reported in the regions O1 s (540–525 eV), Al2p (85–65 eV) and La 3d5/2 (850–830 eV).

Table 2
Comparison of nominal, XPS and EDX composition in atomic% (**mean composition used for 80LaA).

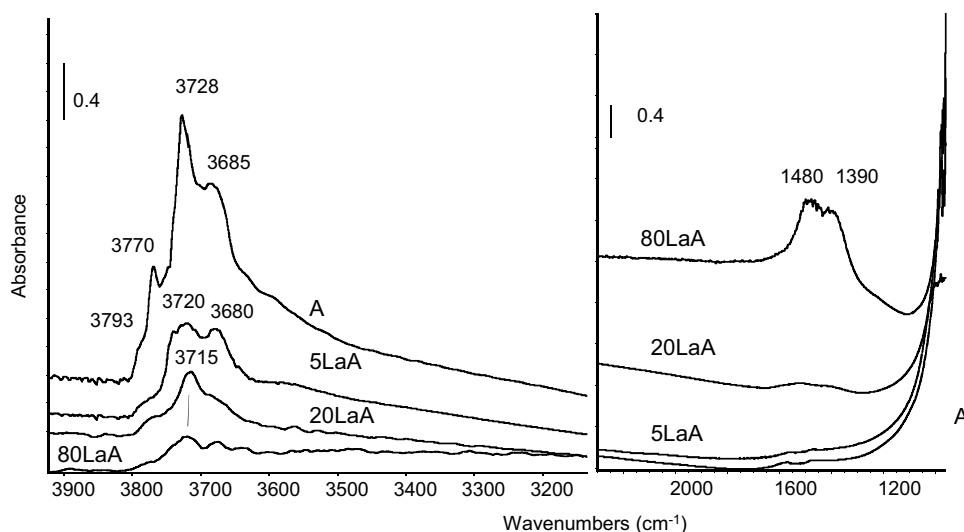| Sample	Nominal composition atomic [%]			XPS composition atomic [%]			EDX composition atomic [%]		
	Al	O	La	Al	O	La	Al	O	La
A	40.0%	60.0%	–	42.1%	57.9%	–	35.4%	64.6%	–
5LaA	39.4%	60.0%	0.6%	41.4%	58.2%	0.5%	33.9%	65.5%	0.6%
20LaA	37.6%	60.0%	2.4%	38.9%	59.5%	1.5%	33.0%	64.7%	2.3%
80LaA**	32.0%	60.0%	8.0%	34.1%	58.7%	7.3%	25.3%	64.2%*	10.5%

Fig. 4. IR spectra of the investigated catalysts after activation in vacuum at 773 K in (left) OH region and (right) 2500–1100 cm^{-1} range with carbonate assignments.

of the 5LaA sample shows a broad and multiple component at 3720 cm^{-1}, another maximum, sharper, at 3680 cm^{-1}, and a weak shoulder at 3790 cm^{-1}. The sharp component at 3770 cm^{-1} present in the spectrum of A has disappeared completely. The spectrum of the 20LaA sample presents a quite sharp peak at 3715 cm^{-1}, with pronounced shoulders near 3780 and 3680 cm^{-1}. Interestingly, the spectrum does not show evident components in the region typical of La-OH groups observed on the surface of La$_2$O$_3$ samples, typi-

cally found in the 3680–3610 cm^{-1} region [38–41]. In the case of the sample 80LaA, the disk has low transmission in the high frequency region, where weak bands at ca. 3715, 3680 and maybe 3620 cm^{-1} can be envisaged. The last one could be due to LaOH groups. The data show that for the 80LaA sample the La(OH)$_3$ phase is decomposed under outgassing at 773 K. It is noted that while after activation in vacuum the A, 5LaA and 20LaA samples appear to be essentially clean, without bands due to surface species except OH

groups, after activation at 773 K the sample 80LaA still shows quite intense bands due to carbonate species (see Fig. 4 right), which can be associated either to surface or to bulk lanthanum carbonates [39,42]. On the other hand, XRD does not reveal the presence of bulk lanthanum carbonates. It has been reported that bulk lanthanum oxycarbonates, $(LaO)_2CO_3$, which exist in different crystal structures, decompose into A-type La_2O_3 in the temperature range 1020–1140 K [43–45]. Thus, we expect that the residual carbonate species observed are not bulk carbonates but strongly adsorbed surface species.

The surface acidity has been studied using IR spectra of adsorbed pyridine (Fig. 5). After outgassing at room temperature (r.t.), pyridine adsorbed on A gives rise to two main 8a band components observed at 1595 cm^{-1} (quite broad) and 1613 cm^{-1}, together with a shoulder near 1620 cm^{-1}. They correspond to a complex 19b band centered at 1446 cm^{-1} with an evident shoulder at higher frequency. After outgassing at 573 K the main 8a band is that observed now at 1622 cm^{-1} with a shoulder evident near 1615 cm^{-1}, while the 19b band is now observed at 1456 cm^{-1}. As discussed elsewhere, the 8a bands at 1622 and 1616–12 cm^{-1} are due to pyridine interacting with low coordination Al cations on the corners and on the edges (or in any case on defects) of the γ-Al$_2$O$_3$ crystals [2,16,17] while pyridine bonded to Na$^+$ impurity cations and to pentacoordinated Al^{3+} ions contribute to the band at ca. 1595 cm^{-1}.

In the case of the 5LaA sample, the presence of Lanthanum causes only slight differences in the spectra of adsorbed pyridine. In particular, the intermediate component after outgassing at r.t. is at a slightly higher frequency, 1598 cm^{-1}, while after outgassing at 573 K the main bands are observed at 1613 cm^{-1} (8a) and 1451 cm^{-1} (19b) with shoulders at higher frequencies. The band at 1598 cm^{-1} could be attributed to pyridine adsorbed on Lanthanum ions acting as Lewis acid sites, in agreement with results reported for pyridine adsorbed on other La-containing oxides [41,46–48]. In the case of the 20LaA sample, two well different pyridine chemisorbed species are found with 8a components at 1614 and 1600 cm^{-1}, assigned to Lewis acidic Al^{3+} and La^{3+} species. The strongest alumina Lewis acid sites seem to have disappeared. In the case of the 20LaA sample only species with the 8a component at $-\nu < 1600$ cm^{-1} (19b component at 1442 cm^{-1}) are observed suggesting that only La^{3+} species act as weak Lewis acid sites. Over this material, pyridine is fully desorbed by outgassing at 523 K.

As discussed elsewhere [49], carbon dioxide is a good probe molecule for the characterization of surface basicity. In Fig. 6, the IR spectra of the adsorbed species arising from the adsorption of CO$_2$ on the 5LaA and 20LaA catalysts are compared. In the case of 80LaA no adsorption of CO$_2$ is found, likely due to the presence of strongly adsorbed carbonates already in the samples outgassed at 773 K. The bands at 1643 cm^{-1}, 1484 cm^{-1} (with 1450 cm^{-1} as a shoulder) and 1236 cm^{-1} observed upon adsorption of CO$_2$ on sample A are due to surface bicarbonate species (C=O asymmetric and symmetric stretching, and OH deformation, respectively [50]). These bands show that over hydroxylated alumina few nucleophilic (basic) hydroxyl- groups exist converting CO$_2$ into bicarbonate species, as discussed elsewhere [2]. The spectrum of adsorbed species is only strongly reduced in intensity by addition of Lanthanum for 5LaA, while it is definitely modified for the 20LaA sample. In this case, the bands due to bicarbonate species broaden and shift to ca. 1630, 1428 and 1229 cm^{-1}, while bands due to carbonate species at ca 1530 and 1350 cm^{-1} (asymmetric and symmetric C=O stretching), possibly with further components in the region near 1630 cm^{-1}, are formed. This shows that La addition first inhibits the basic sites of alumina that produce bicarbonate species by CO$_2$ adsorption, then, at larger loadings, provides new basic and nucleophilic sites for CO$_2$ adsorption. The data are in rough agreement with those reported recently for similar samples by Feist and Hill [51].

Sample	T [K]	X C$_2$H$_6$O	S CH$_2$CH$_2$	S CH$_3$CH$_3$	S C$_4$	S DEE
A	623	100%	96.7%	1.9%	1.4%	0.0%
	673	100%	97.2%	1.6%	1.2%	0.0%
	723	100%	98.0%	1.5%	0.3%	0.0%
5LaA	623	100%	97.2%	0.4%	1.5%	1.0%
	673	100%	98.4%	0.4%	1.0%	0.2%
	723	100%	98.2%	0.4%	1.0%	0.5%

3.1.7. Temperature programmed desorption of isopropanol (IPA-TPD)

In Fig. 7, isopropanol TPD profiles, recorded over the four catalysts, are shown. The strong peak observed for $m/z = 41$ due to propene shifts progressively to higher temperature at increasing lanthanum loading from 438 K for A, to ca 473 K for 5LaA, ca 523 K for 20LaA and to 598 K for 80LaA, with a corresponding progressive decrease of the intensity of the peak. Desorption of intact isopropanol is essentially negligible.

These data show that the addition of lanthanum causes a progressive decrease of the number and strength of the acid sites, which are considered responsible for propene formation.

3.2. Catalytic activity

3.2.1. Ethanol temperature programmed surface reaction (TPSR)

Ethanol TPSR curves on the four catalysts are reported in Figs. 4S–7S. On pure alumina A (Fig. 4S) the conversion of ethanol starts at 540 K producing diethylether whose desorption peaks at 620 K. The production of ethylene starts at 580 K and grows progressively until 670 K. The amounts of observed by-products are essentially zero. An increased La loading produces a shift of ethanol conversion towards higher temperatures, i.e. from 550 K for 5LaA to 680 K for 80LaA (Fig. 5S–7S), and to the appearance of several byproducts (acetaldehyde, CO, CO$_2$ and methane).

The data show that dehydrating activity is predominant for all samples, but starts at increasing temperatures for increased La loadings, as found also by IPA-TPD. Additionally, the production of diethylether (DEE) progressively vanishes at increasing lanthanum loading, ethylene becoming the only dehydration product. The dehydrogenating activity to acetaldehyde becomes relevant for sample 80LaA, where however, the dehydration activity is still dominant. These findings are in line with the activity reported for pure lanthana, where low amounts of acetaldehyde are formed from ethanol conversion together with ethylene and reaction occurs at higher temperature [52].

3.2.2. Steady-state ethanol reaction tests

The data concerning the catalytic activity in steady-state ethanol conversion experiments are summarized in Fig. 8, and in Table 3. The mass balance is essentially always fulfilled in these conditions.

The performance of sample A in ethanol dehydration experiments is slightly different from that already reported for the same material, uncalcined [6]. At moderate temperature (473–523 K), conversion is also moderate (up to 0.74) and DEE is produced with high selectivity. The maximum yield to DEE is 68% at 523 K. At 623 K, conversion is still incomplete (0.85) but selectivity to ethylene is now very high (84.8%), while at higher temperature (623–673 K) conversion is total and yield to ethylene is >0.967. Ethylene yield is limited by the formation of ethane and C4 hydrocarbons.

At increasing La loadings, the conversion of ethanol shifts progressively to higher temperatures. In parallel, the maximum yield to diethyl ether progressively decreases and shifts to higher temperatures, while the ethylene yield curve also shifts to higher temperatures.
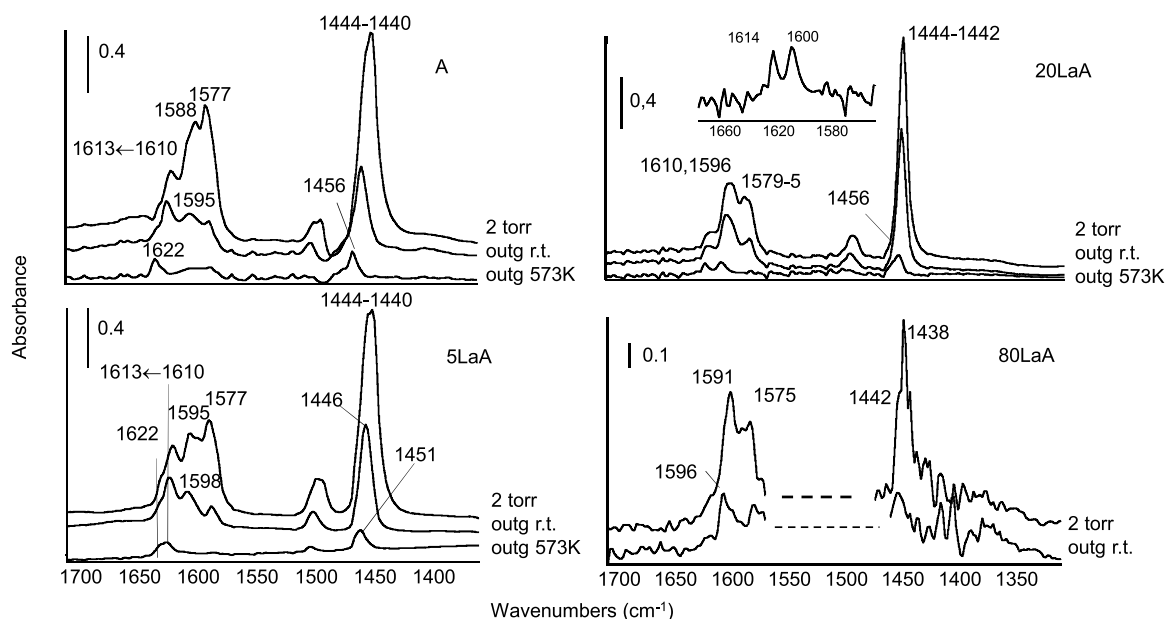
Fig. 5. IR spectra of pyridine adsorption for the investigated catalysts. In each case, spectra of pyridine adsorbed at r.t., after evacuation at r.t. and at 573 K are reported.
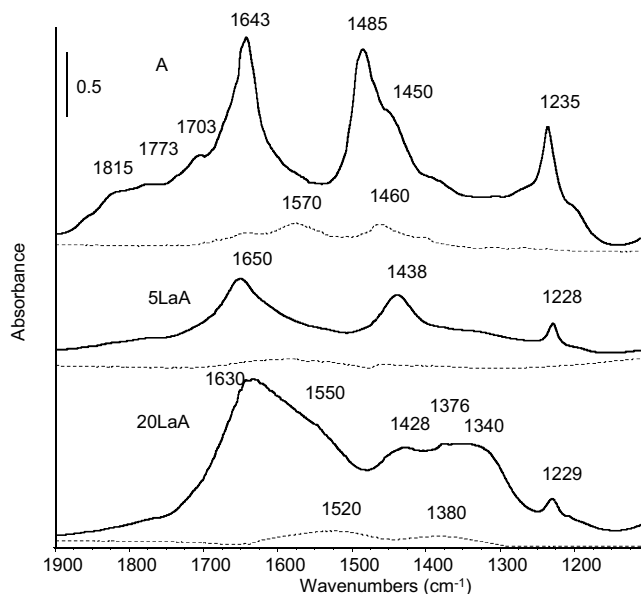

Fig. 6. IR spectra of CO_2 adsorption at r.t. (solid line) and after evacuation at 423 K (dashed line).

Only in the case of 5LaA, the ethylene yield is still very high at high ethanol conversion, with ethylene yields of 97–98.5% in the temperature range 623–773 K. In this temperature range, the ethylene yield is the same (taking into account experimental error) and almost total on A and 5LaA. The small amounts of by-products are slightly different on A (ethane 1.5–2%, 1- and 2-butenes ca. 1–1.5%) and on 5LaA (ethane 0.4%, 1- and 2-butenes ca 1–1.5%, DEE 0.5–1%)

In contrast, the maximum ethylene yield decreases very much at higher La loadings, with the formation of significant amounts of by-products such as acetone, propene and C_4 hydrocarbons.

3.2.3. Characterization of spent catalysts

In Fig. 7S, images of the spent catalysts are reported. It is evident that carbonaceous matter is grown over them, and that the spent A catalyst has the darkest colour while the spent sample 80LaA has the lightest one. Correspondingly the spent sample A indeed shows the strongest absorption in the visible, as well as in the UV region (Fig. 2S). A continuous absorption is observed in the visible range with a peak in the UV region at 330 nm. The spent samples 5LaA and 20LaA show definitely weaker absorptions, markedly different from each other. In agreement with the reddish colour, the spent sample 20LaA absorbs more than spent 5LaA in the higher energy part of the visible and in the UV, and less in the lower energy part of the visible. Sample 80LaA has the weakest absorption in the UV and visible ranges. In all cases, no evident peaks are observed in the visible, and this suggests that the nature of carbon matter is different here than that observed after ethanol conversion over protonic zeolites [19], where definite peaks were evident.

Temperature-programmed oxidation (O_2-TPO) of spent A and 5LaA catalysts after ethanol conversion experiments have also been
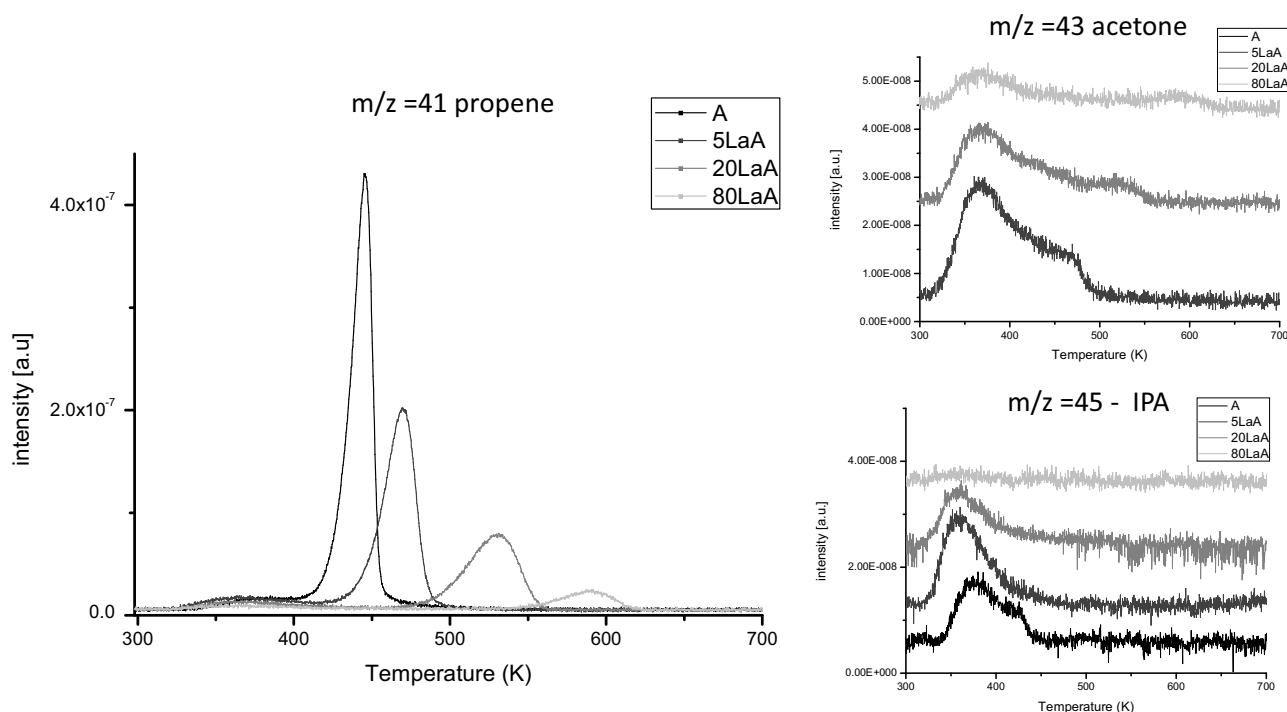
Fig. 7. IPA-TPD results for the investigated catalysts. The profiles for $m/z = 41$ (propylene), $m/z = 43$ (acetone) and $m/z = 45$ (isopropanol) are reported as a function of temperature.
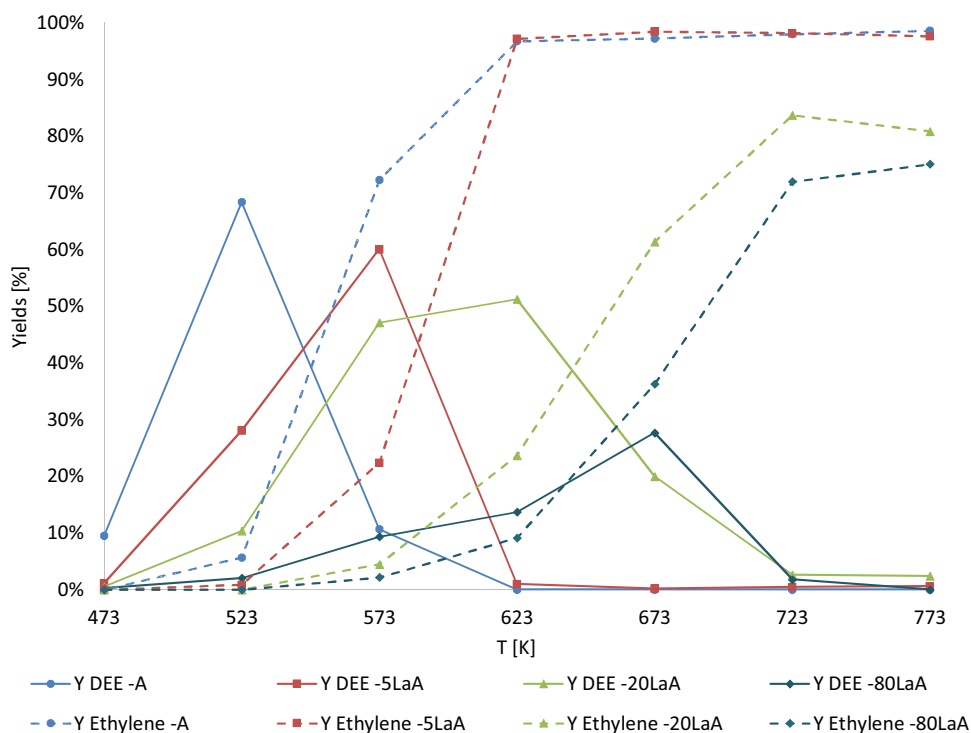

Fig. 8. Results of flow reactor study for the investigated catalysts in terms of ethylene yield (Y Ethylene) and diethylether yield (Y DEE) as a function of reaction temperature.

carried out (Fig. 9). Indeed the amount of CO_2 evolved from spent 5LaA sample is definitely lower than that evolved from spent A, while the amount of CO evolved from the two catalysts is similar. These data show that the amount and type of carbon matter formed on the samples A and LaA, which have similar excellent catalytic activity for producing ethylene at T 623–773 K, is different.

4. Discussion

The samples considered in this paper were prepared by incipient wetness impregnation technique using a well-known alumina support which was the object of previous characterization studies [16,18]. Taking into account that the theoretical monolayer was evaluated in previous papers [53,54] to be a little more than 5La
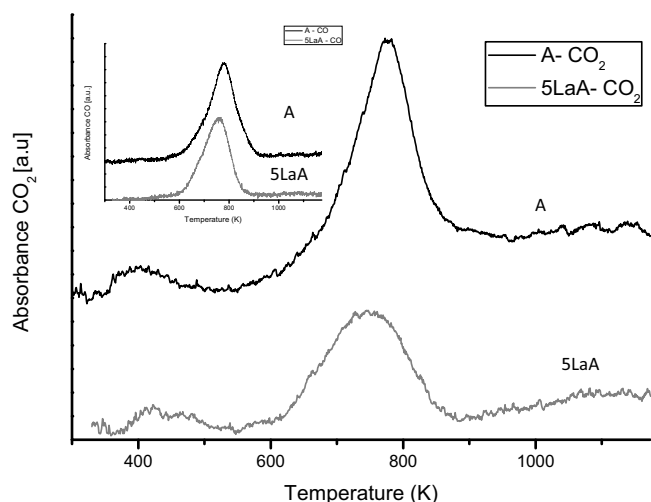
Fig. 9. CO_2 absorbance as a function of temperature during O_2-TPO for A and 5LaA catalysts. In the inset the CO absorbances recorded for both catalysts are shown.

atoms per nm^2, the amount of lanthanum loaded (Table 1) can be evaluated. A small fraction of the theoretical monolayer is achieved in 5LaA, while a little less than a monolayer is estimated for 20LaA, and more than four monolayers for sample 80LaA.

For 80LaA, all data show a strong interaction between the alumina and the impregnated phase. XRD, IR and XPS show not only the formation of $La(OH)_3$ but also the formation of a mixed oxide phase (the perovskite $LaAlO_3$). The strong interaction is also evident in the TEM images that show, together with La-rich particles, a strong modification of the alumina-rich particle shape, which became rounded. The XRD pattern can also be interpreted supposing that a partial amorphization of alumina also occurred. Looking at phase equilibria of the La_2O_3-Al_2O_3 system, the formation of two intermediate phases between La_2O_3 (which is stable up to 2300 K in the A-type rare earth oxide phase) and α-Al_2O_3 (Corundum) is seen, i.e. the perovskite $LaAlO_3$ and the beta-alumina phase $LaAl_{11}O_{18}$ [55]. Some authors report also the formation of metastable crystalline phases in the system [56–59]. Our study shows the high reactivity of γ-Al_2O_3 with La_2O_3 or its precursors (such as La hydroxide, nitrate or oxynitrate), producing $LaAlO_3$ at 1023 K. Previous studies indeed showed that crystallization of $LaAlO_3$ can occur already at 873 K from co-precipitated powders [60], although usually higher temperatures are needed (973–1173 K [61,62]), but their formation seems much easier than that of $LaAl_{11}O_{18}$ and of α-Al_2O_3, which occur at higher temperature [63].

These findings indicate that even small amounts of Lanthana indeed tend to stabilize γ-Al_2O_3 against sintering and loss of surface area (samples 5LaA and 20LaA), as it has been reported by several studies [3,4]. The formation of bulk lanthanum-containing phases can instead cause the reaction of γ-Al_2O_3 at moderate temperatures, with the formation of bulk $LaAlO_3$, and an important decrease of surface area.

Characterization data show that the 80LaA sample is largely dehydroxylated by outgassing at 773 K and fully lost the strong Lewis acidity of alumina. Weak Lewis sites due to La^{3+} ions and significant basicity associated to the strong bonding of CO_2 in the form of strongly adsorbed or even bulk-like carbonates are observed. IPA-TPD confirms a strong reduction in acidity with respect to alumina (small propylene evolution only at 590 K) with the appearance of some basicity (acetone evolution). The activity in converting ethanol is also strongly reduced but, maybe surprisingly, diethylether first and ethylene later are still largely the main products. We must however point out that IPA-TPD experiments have been performed on samples pretreated at 523 K and catalytic exper-

iments in ethanol conversion were performed on samples without any pre-treatment. Thus, in both cases the experiments have been performed on carbonate-covered 80LaA samples. This implies that the strong basic sites of the catalysts where indeed neutralized by surface carbonates. It is likely that high-temperature pre-treated samples would reveal a strong basic behaviour.

The characterization of the 20LaA sample still shows γ-Al_2O_3 as the only phase without any La-rich phase formed. This agrees with published data for a similar sample [64]. The data arising from TEM and FTIR spectroscopy indicate that the surface structure of this sample, whose lanthana amount is near monolayer coverage, is strongly modified. Lanthanum species appear to be well dispersed in TEM experiments, with a resulting decrease of the number of the OH groups detected by IR spectroscopy. In parallel, IR spectra of adsorbed pyridine reveal the full disappearance of the strongest Al^{3+} Lewis acid sites of alumina and the persistence of the medium strength Al^{3+} Lewis acid sites, with the concomitant predominance of La^{3+} weak Lewis acid sites. Medium-strength basic sites are also apparent, together with the weaker basic sites of alumina: in fact, both carbonates and bicarbonates form by CO_2 adsorption, but both disappear by outgassing at 423 K. Also in this case, IPA-TPD confirms a significant reduction in acidity with respect to alumina (i.e. smaller propylene evolution at higher temperature, ca 523 K). The activity in converting ethanol is reduced but, maybe surprisingly, diethyl ether first and ethylene later are still largely the main products. In this case, IR spectroscopy data suggest that both IPA-TPD and catalytic ethanol conversion experiments were performed with a nearly clean surface.

For sample 5LaA, the data suggest that Lanthanum ions spread over the alumina surface, covering it only partially. In fact, XRD and FT-IR skeletal data do not show modifications of the alumina. Interestingly, the surface area of 5LaA is essentially the same (taking in account the experimental error) as that of A. The TEM analysis does not reveal any relevant modification of particle size and shape of alumina by La doping. The original prismatic particles appear to be unmodified.

The surface chemical characterization shows that over this sample the amount of the surface OH groups is markedly reduced, while the OH group responsible for the band at 3767 cm^{-1} is totally absent. In fact, this is what occurs in most cases when alumina is used as a support, showing a particularly high reactivity or presence of this family of surface OH groups [2]. On the other hand, the peak at 3728 cm^{-1} is also absent or remarkably decreased in intensity. According to a recent publication, this band could be due, at least in part, to the SiOH silanol groups associated to Puralox alumina (as on any other aluminas) due to a small amount of silica impurities (Si 52 ppm) [18]. The other features in the OH stretching spectrum are still observed, although also decreased in intensity. The presence of lanthanum species on 5LaA results also in reduced amount of bicarbonates formed on the surface upon CO_2 adsorption. Pyridine adsorption indicates that, besides the presence of some La^{3+} cations acting as weak Lewis acid sites, the impregnation with lanthanum caused inversion of the amounts of Al^{3+} cations responsible for the pyridine species absorbances at 1622 and 1613 cm^{-1}. After La addition, when pyridine is outgassed at 573 K the band at 1613 cm^{-1} is stronger than that at 1622 cm^{-1}, while the reverse is true for bare alumina. These data provide evidence of specific interactions of La^{3+} cations and the related O^{2-} counter-anions produced by impregnation/calcination. Lanthanum cations would interact specifically with the alumina basic sites (those producing bicarbonate ions from CO_2 adsorption) while the O^{2-} counter-anions would interact specifically with the strongest Al^{3+} Lewis acid sites (those involved in the 1622 cm^{-1} band), enlarging their coordination thus converting them into the "medium Lewis acidity" Al^{3+} Lewis acid sites (those involved in the 1613 cm^{-1} band). In some way, La^{3+} cations and O^{2-} counter-anions essentially partially neutralize the

strongest Lewis acid-base couples of alumina. This confirms the hypothesis that the most active alumina Lewis acid sites are Al^{3+} cations (probably in trigonal coordination) and OH anions responsible for the band at 3767 cm^{-1} [2].

The catalytic IPA-TPD study confirms that the Lewis acidity of the 5LaA sample is definitely lower than that of alumina, resulting in a shift to higher temperature of the peak associated with the propylene production. In addition, the amount of produced propylene is significantly decreased. On the other hand, the production of acetone is very low, thus suggesting that basicity is very weak in terms of sites strength and/or amount.

The catalytic activity in ethanol conversion of 5LaA is also reduced with respect to that of the bare support. In the TPSR experiments, it is very clear that the production of ethylene is shifted to higher temperatures by nearly 50 K. The same effect is found considering the steady-state step flow reactor experiments. However, this catalyst retains the ability of alumina to produce very high yields in ethylene, >98%, although only at higher temperatures. The selectivities to byproducts observed on 5LaA at full ethanol conversion are slightly different from those observed on alumina, with a lower selectivity to propane and a slight production of diethyl ether at very high conversion. Interestingly, the selectivity to diethyl ether at lower conversion is much higher on 5LaA than on A: in fact over LaA at 573 K the conversion of ethanol is 82% and the selectivity to diethylether is 72.8% (corresponding to a yield of 60%), while over A at the same temperature (573 K) the conversion is slightly higher (85.2%) but the selectivity to diethylether is much lower (12.5%, corresponding to a 10.6% yield) with ethylene already being the main product. This suggests that the alumina Lewis acid sites are located near the basic sites generated by lanthanum oxide species in the case of 5LaA, and this would favor the formation of diethylether as discussed elsewhere [65].

However, at higher temperature ethanol conversion is complete also over 5LaA and ethylene selectivity is also very high. The activity/selectivity of 5LaA and alumina are essentially the same at 673 K, 5LaA being perhaps slightly better than alumina. However, the amount of residual carbon species after the catalytic experiments is significantly higher on A than on 5LaA. Thus, deactivation by coking in prolonged experiments would be smaller on 5LaA than on alumina, justifying the addition of lanthanum to improve the alumina stability under these conditions.

5. Conclusions

The present study allowed us to confirm that the addition of lanthanum to γ-Al$_2$O$_3$ in amounts well below or close to the theoretical monolayer stabilizes alumina with respect to sintering and loss of surface area, as well as against carbon laydown. However, when higher amounts of lanthanum oxide are used (equivalent to ~4.7 theoretical monolayers in our case) the formation of bulk lanthanum oxide-containing phases can instead cause the reaction of γ-Al$_2$O$_3$ at moderate temperature, with the formation of bulk LaAlO$_3$ and a significant decrease of surface area. In this case, the acid properties of alumina are fully lost and the surface is covered by strongly bonded carbonates at least if activation is performed at temperatures not higher than 773 K. The catalytic activity is much reduced with respect to alumina, but diethylether and ethylene are still the main products. It is likely that this material will display strong basicity after outgassing at higher temperatures.

For a coverage similar to that of a theoretical monolayer (0.8 of a monolayer here), lanthanum species spread on the surface and neutralize partially the acido-basic properties of alumina. Under these conditions a new family of basic sites is produced, which have moderate basicity. The activity is definitely lowered with respect to

alumina, but diethylether and ethylene are still the main products. The typical features of a basic catalyst do not appear.

When the loaded lanthanum oxide species are in the range of a small fraction of the monolayer (0.2 here), partial neutralization of the acido-basic properties of alumina is observed. The catalyst retains significant strong Lewis acidity and some new basic centers. The surface characterization data suggest that the La^{3+}-O^{2-} couples interact specifically with the strongest acido-basic sites of alumina reducing the Lewis acidity but providing strongest acido-basic couples. These catalysts are less active in ethanol dehydration than alumina but more selective to diethylether at partial conversion. They are also equally or more selective to ethylene at high conversion, with respect to ethylene overconversion products. In addition, they produce less carbonaceous material during reaction. Thus, they are good candidates for application as catalysts for the production of (bio)ethylene from (bio)ethanol dehydration.

Notes

In the present paper with the common term bicarbonate, we always refer to hydrogen carbonate according to IUPAC nomenclature.

Appendix A. Supplementary data

Supplementary data associated with this article can be found, in the online version, at http://dx.doi.org/10.1016/j.apcatb.2016.07.010.

References

[1] Y. Ono, H. Hattori, Solid Base Catalysis, Tokyo Institute of Technology Press, 2011, pp. 91–96.
[2] G. Busca, Adv. Catal. 57 (2014) 319–404.
[3] B. Béguin, E. Garbowski, M. Primet, Appl. Catal. 75 (1991) 119–132.
[4] P. Alphonse, B. Faure, Microporous Mesoporous Mater. 196 (2014) 191–198.
[5] M. Li, D. Weng, X. Wu, J. Wan, B. Wang, Catal. Today 201 (2013) 19–24.
[6] C.H. Bartholomew, R.J. Farrauto, Fundamentals of Industrial Catalytic Processes, 2nd ed., Wiley, 2005, p. 719.
[7] E.D. Banús, M.A. Ulla, E.E. Miró, V.G. Milt, Structured Catalysts for Soot Combustion for Diesel Engines, in Diesel Engine? Combustion, Emissions and Condition Monitoring, Saiful Bari InTech, 2013, pp. 117–143.
[8] Y. Li, Catalyzed soot filter manufacture and systems, US 8114354 B2 to Basf Corporation (2012).
[9] M.C. Sánchez- Sánchez, R.M. Navarro, J.J.G. Fierro, Catal. Today 129 (2007) 336–345.
[10] G. Garbarino, C. Wang, I. Valsamakis, S. Chitsazan, P. Riani, E. Finocchio, M. Flytzani-Stephanopoulos, G. Busca, Appl. Catal. B: Environ. 174–175 (2015) 21–34.
[11] N. Habibi, M. Rezaei, N. Majidian, M. Andache, J. Energy Chem. 23 (2014) 435–442.
[12] J. Mazumder, H.I. de Lasa, Appl. Catal. B: Environ. 168–169 (2015) 250–265.
[13] A. Limayem, S.C. Ricke, Prog. Energy Combust. Sci. 38 (2012) 449–467.
[14] M. Balat, Energy Convers. Manag. 52 (2011) 858–875.
[15] J. McKetta, Chemical Processing Handbook, Wiley, 1993, pp. 786–789.
[16] T.K. Phung, A. Lagazzo, M.Á. Rivero Crespo, V. Sanchez Escribano, G. Busca, J. Catal. 311 (2014) 102–113.
[17] T.K. Phung, C. Herrera, M.Á. Larrubia, M. García-Diéguez, E. Finocchio, L.J. Alemany, G. Busca, Appl. Catal. A: Gen. 483 (2014) 41–51.
[18] G. Garbarino, I. Travi, M. Pani, M.M. Carnasciali, G. Busca, Catal. Commun. 70 (2015) 77–81.
[19] T.K. Phung, L. Proietti Hernandez, A. Lagazzo, G. Busca, Appl. Catal. A: Gen. 493 (2015) 77–89.
[20] J. Sun, Y. Wang, ACS Catal. 4 (2014) 1078–1090.

[21] J.M.R. Gallo, J.M.C. Bueno, U. Schuchardt, J. Braz. Chem. Soc. 25 (2014) 2229–2243.
[22] Pearson's Crystal Data – Crystal Structure Database for Inorganic Compounds (on DVD), Release 2014/15, ASM International, The Material Information Society.
[23] G. Busca, Catal. Today 226 (2014) 2–13.
[24] D. Zheng, J. Shi, X. Lu, C. Wang, Z. Liu, C. Liang, P. Liu, Y. Tong, CrystEngComm 12 (2010) 4066–4070.
[25] G. Jia, C. Zhang, C. Wang, L. Liu, C. Huang, S. Ding, CrystEngComm 14 (2012) 579–584.
[26] J. Haeberle, K. Henkel, H. Gargouri, F. Naumann, B. Gruska, M. Arens, M. Tallarida, D. Schmeißer, Beilstein J. Nanotechnol. 4 (2013) 732–742.
[27] C.E. Moffatt, B. Chen, D.M. Wieliczka, M.B. Kruger, Solid State Commun. 116 (2000) 631–636.
[28] Y. Kameshima, A. Yasumori, K.J. Okada, Surf. Sci. Soc. Jpn. 21 (2000) 481–487.
[29] L.P. Haack, J.E. deVries, K. Otto, M.S. Chatta, Appl. Catal. A: Gen. 82 (1992) 199–214.
[30] X. Chen, Y. Liu, G. Niu, Z. Yang, M. Bian, A. He, Appl. Catal. A: Gen. 205 (2001) 159–172.
[31] M. Ferrandon, E. Björnbom, J. Catal. 200 (2001) 148–159.
[32] S. Mickevičius, S. Grebinskij, V. Bondarenka, B. Vengalis, K. Sliuziene, B.A. Orlowski, V. Osinniy, W. Drube, J. Alloys Compd. 423 (2006) 107–111.
[33] Z. Boukha, L. Fitian, M. López-Haro, M. Mora, J.R. Ruiz, C. Jiménez-Sanchidrián, G. Blanco, J.J. Calvino, G.A. Cifredo, S. Trasobares, S. Bernal, J. Catal. 272 (2010) 121–130.
[34] J. Zheng, X. Ren, Y. Song, X. Ge, React. Kinet. Catal. Lett. 97 (2009) 109–114.
[35] K. Ikkour, D. Sellam, A. Kiennemann, S. Tezkratt, O. Cherifi, Catal. Lett. 132 (2009) 213–217.
[36] K. Zhang, G. Zhou, J. Li, K. Zhen, T. Cheng, Catal. Lett. 130 (2009) 246–253.
[37] K.H. Hadjiivanov, Adv. Catal. 57 (2014) 99–318.
[38] A.A. Tsyganenko, J. Lamotte, J.P. Gallas, J.C. Lavalley, J. Phys. Chem. 93 (1989) 4179–4183.
[39] B. Klingenberg, M.A. Vannice, Chem. Mater. 8 (1996) 2755–2768.
[40] A. Paulidou, R.M. Nix, Surf. Sci. 470 (2000) L104–L108.
[41] O.V. Manoilova, S.G. Podkolzin, B. Tope, J. Lercher, E.E. Stangland, J.M. Goupil, B.M. Weckhuysen, J. Phys. Chem. B 108 (2004) 15770–15781.
[42] R. Sarbajna, A.S. Devi, K. Purandhar, M.V. Suryanarayana, Int. J. Chem. Tech. Res. 5 (2013) 2810–2820.
[43] B. Bakiza, F. Guinnetona, M. Araba, A. Benlhachemi, J.R. Gavarria, Mor. J. Condens. Matter 12 (2010) 60–67.
[44] O. Yamaguchi, K. Sugiura, K. Shimizu, Zeitschrift für anorganische und allgemeine Chemie 514 (1984) 205–212.
[45] A. Olafsen, A.-K. Larsson, H. Fjellvåg, B.C. Hauback, J. Solid State Chem. 158 (2001) 14–24.
[46] A. Vazquez, T. Lopez, R. Gomez, X. Bokhimi, A. Morales, O. Novaro, J. Solid State Chem. 128 (1997) 161–168.
[47] A. Vazquez, T. Lopez, R. Gomez, X. Bokhimi, J. Mol. Catal. A: Chem. 167 (2001) 91–99.
[48] G.A.H. Mekhemer, Phys. Chem. Chem. Phys. 4 (2002) 5400–5405.
[49] G. Busca, Chem. Rev. 110 (2010) 2217–2249.
[50] G. Busca, V. Lorenzelli, Mater. Chem. 7 (1982) 89–126.
[51] B.J. Feist, J.M. Hill, Energy Fuels 29 (2015) 6049–6056.
[52] M.P. Rosynek, R.J. Koprowski, G.N. Dellisante, J. Catal. 122 (1990) 80–94.
[53] M. Bettman, R.E. Chase, K. Otto, W.H. Weber, J. Catal. 117 (1989) 447.
[54] Z. Boukha, L. Fitian, M. López-Haro, M. Mora, J.R. Ruiz, C. Jiménez-Sanchidrián, G. Blanco, J.J. Calvino, G.A. Cifredo, S. Trasobares, S. Bernal, J. Catal. 272 (2010) 121–130.
[55] L. Li, Z. Tang, W. Sun, P. Wang, J. Mater. Sci. Technol. 15 (1999) 439–443.
[56] M. Mizuno, M. Berjoan, J.P. Coutures, M. Foex, Y. Kyokaishi, J. Ceram. Soc. Jpn. 82 (1974) 631–636.
[57] M. Mizuno, T. Yamada, T. Noguchi, Y. Kyokaishi, J. Ceram. Soc. Jpn. 83 (1975) 90–96.
[58] O. Yamaguchi, K. Sugiura, A. Mitsui, K. Shimizu, J. Am. Ceram. Soc. 68 (1985) 44–45.
[59] T.S. Key, B. Crist Jr., J. Am. Ceram. Soc. 88 (2005) 191–195.
[60] L. Djoudi, M. Omari, N. Madoui, EPJ Web Conf. 29 (2012) 00016.
[61] C.L. Kuo, Y.H. Chang, M.C. Wang, Ceram. Int. 35 (2009) 327–332.
[62] P.N. Plassmeyer, K. Archila, J.F. Wager, C.J. Page, ACS Appl. Mater. Interfaces 7 (2015) 1678–1684.
[63] G.C.C. da Costa, R. Muccillo, Mat. Sci. Forum 530-531 (2006) 649–654.
[64] Y. Nishio, M. Ozawa, J. Ceram. Soc. Jpn. 116 (2008) 1295–1298.
[65] T.K. Phung, G. Busca, Catal. Commun. 68 (2015) 110–116.